2024 IEEE/RSJ International Conference on Intelligent Robots and Systems (IROS)
October 14-18, 2024. Abu Dhabi, UAE

Towards Robotised Palpation for Cancer Detection through Online Tissue Viscoelastic Characterisation with a Collaborative Robotic Arm

Luca Beber[1,2], Edoardo Lamon[1,3], Giacomo Moretti[4], Daniele Fontanelli[4], Matteo Saveriano[4], Luigi Palopoli[1]

***Abstract*— This paper introduces a new method for online estimating the penetration of the end-effector and the viscoelastic properties of a soft body, through palpation exams using a collaborative robotic arm. The estimator is based on the dimensionality reduction method that simplifies the nonlinear Hunt-Crossley model. In addition, in our algorithm, the model parameters can be found without a force sensor, leveraging only the robotic arm controller data. An extended Kalman filter is employed to achieve online estimation, which embeds the dynamic contact model. The algorithm is tested with various types of silicone, a material that resembles biological tissues, including samples with hard intrusions to simulate cancerous cells within a softer tissue. The results indicate that this technique can accurately determine the model parameters and estimate the penetration of the end-effector into the soft body. These promising preliminary results demonstrate robots' potential to be an effective tool for early-stage cancer diagnostics.**

I. INTRODUCTION

Palpation screening exams are noninvasive and inexpensive procedures that can help to detect cancer or other abnormalities at early stages when they are most treatable. During the exam, healthcare professionals use their hands to feel for lumps, masses, or enlarged lymph nodes that could be signs of cancer. However, the efficacy of the visit highly depends on the healthcare provider's experience and skill in feeling for abnormalities, especially when they are small, deep within the body, or located in soft tissues. Robotised palpation exams have the potential to reduce the subjectivity inherent in human performance by standardising the procedure. Therefore, this technology could improve the reliability of the results, and reduce the influence of the examiner's experience. Another important benefit of robotised palpations is the realisation of exams in geographical areas that are not covered by adequate health-care services.

In the past decades, several robotic palpation systems have been introduced for the detection of hard bodies within soft tissues, leveraging artificial tactile sensors and sensorised probes [1]–[3], and mechanical property characterisation with inverse finite element estimation methods [4], [5]. A key element of any robotised palpation system is a solution for online estimation of biological tissue parameters. Indeed, palpation exams require to locate stiffer points on the body [6], [7]. The same technology is also important for other medical applications. For example, in robot-assisted minimally invasive surgery (RMIS), haptic feedback can be implemented by accurately reconstructing the force on the end-effector [8]. Body-related information can also be applied to enable force-controlled navigation of a probe along the surface of the human body. In this case, it is important to ensure adequate levels of safety by regulating the force in contact with rigid body parts and accidental motions of the patient [9]–[11].

Different models suitable for estimation can be adopted to characterise soft tissues. Pappalardo et al. [12] showed that linear models, such as the Kelvin-Voigt or Maxell models, have limitations as they do not account for the geometry of the contact surface between the end-effector and the soft body. A better-suited choice is the nonlinear Hunt-Crossley (HC) model, which describes the tridimensionality of the contact and reconstructs the force on the end-effector with higher precision [13]. Such models are used in combination with different estimation methods, such as non-linear square regression [14], [15] and Kalman filters [12], [16]–[18].

Despite their promising results, the aforementioned approaches share two common limitations. The first is that the penetration depth is assumed known [16], which is unrealistic in real-life applications. During a palpation test, there is hardly any way to measure penetration. To overcome this problem, Roveda et al. [17] propose an approach phase in which the end-effector is slowly moved until contact with the body surface occurs. This solution is applicable within experimental settings, where the surface of the palpated object remains constant over time. However, this situation is very unlikely for medical examinations. For example, in the palpation of a person's abdomen, its surface is regularly inflated and deflated while breathing. The second limitation arises from the reliance on highly precise force sensors for the estimation. Such devices are expensive and prone to damage. Besides, they require a regular calibration, which reduces the usability of the device.

To overcome the limitations above, we propose in this paper a method capable of estimating at the same time the penetration inside the body and the parameters of the model. This is possible thanks to the use of the dimensionality reduction method that estimates the exponential term of the Hunt-Crossley equation knowing the shape of the end-effector [19]. In addition, we introduce a dynamical model

We acknowledge the support of the MUR PNRR project FAIR - Future AI Research (PE00000013).

[1]Department of Information Engineering and Computer Science, Università di Trento, Trento, Italy. luca.beber@unitn.it

[2]DRIM, Ph.D. of national interest in Robotics and Intelligent Machines.

[3]Human-Robot Interfaces and Interaction, Istituto Italiano di Tecnologia, Genoa, Italy.

[4]Department of Industrial Engineering, Università di Trento, Trento, Italy.

that links the dynamics of the robotic arm, the end effector position, and the soft surface mechanical behaviour. The combined use of dimensionality reduction and dynamical model allows us to: i) find the amount of penetration ensuring a fast convergence of the model parameters, ii) avoid direct force measurements.

The method is evaluated with a robotic arm equipped with a spherical end-effector and four different silicone samples, two of which contained stiffer material to simulate the presence of a foreign mass. The experiments objective is to estimate in real time the viscoelastic model parameters of the specimen and the correct amount of penetration. Moreover, the force reconstructed with the estimated data has been compared with the one registered by the force torque sensor. Our results show that the package of solutions proposed in the paper reduces the complexity of the system and enhances its physical robustness without any negative impact on the accuracy of the measurements.

II. METHODS

In this section, first, the contact models used to characterise the soft body will be presented; then two different estimation strategies (with and without force sensing) will be illustrated. Finally, we will briefly summarise the use of the extended Kalman filter. One of the simplest ways to describe the interaction between a hard indenter and a soft deformable body is the Kelvin-Voigt (KV) model. This model is popular because, despite its simplicity, it describes an approximation of the contact dynamics. The soft body is treated as an ideal viscoelastic material and contact is considered punctual. The force generated by the soft body is modelled by the combination of a linear spring and a damper acting in parallel, and it can be written as

$$F_M(d) = \begin{cases} k_M d + c_M \dot{d}, & d \geq 0, \\ 0 & d < 0, \end{cases} \tag{1}$$

where $F_M(d)$ is the force generated by the material, d is the penetration inside the body, $\dot{d}$ is the velocity of penetration, k_M is the stiffness of the body and c_M is the damping. Several studies have shown that the model is inaccurate since it does not capture important nonlinear effects when the contact surface cannot be reduced to a point. For this reason, nonlinear models such as the Hunt-Crossley (HC) model are preferable [12], [14]. The HC model is energetically coherent and exposes an explicit dependence between the damping term and the penetration depth. However, the presence of an unknown exponential term makes the estimation very difficult.

If the shape of the end-effector is known, the contact can be described using the dimensionality reduction method (DRM) [19]. In our previous work, we showed that using a robotic arm and an indenter of known shape, the static force can be reconstructed precisely [20]. In this work, the model was modified to include the dynamic response of the material. The idea behind the DRM is that the forces generated by a three-dimensional contact between an axial symmetric indenter and a surface can be computed using

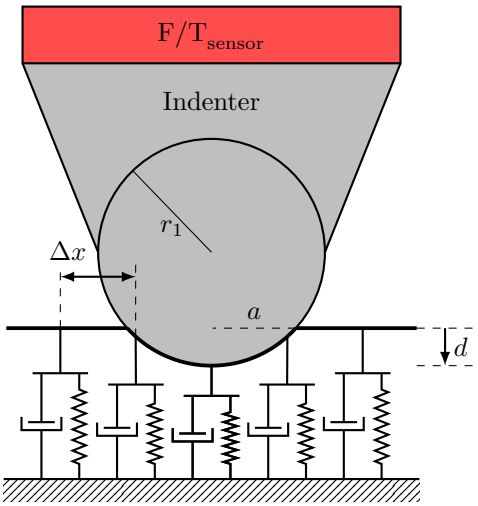

Fig. 1. Schematic of a spherical indenter in constant with a viscoelastic half-plane. Δx is the distance between the viscous elements, a represents half of the projection of the circle's portion in contact, d is the maximum penetration and r_1 is the equivalent radius of the sphere in the viscoelastic halfplane.

the 2D projection onto a plane. For instance, the contact between a sphere, with radius r, and a surface can be studied by limiting the analysis to the contact between a circular arc, with radius $r_1 = r/2$ [19], and a set of parallel mass-damper elements spaced out of a tiny quantity Δx. The deformation of each element is dependent on the contact point between the indenter and the material. In the case of a spherical indenter, the central elements are deformed more than the elements on the borders, as shown in Fig. 1. In this study, we will focus on incompressible materials (Poisson ratio $\nu = 0.5$), i.e. materials for which the volume does not change. Such materials include biological tissues but also silicones [21]. The viscoelastic formulation with DRM can be divided into two subproblems: the purely elastic and the purely viscous. In the purely elastic case, analysed in [20], the contribution of a single spring is

$$f_{M,i} = 4G d_i \Delta x, \tag{2}$$

where $f_{M,i}$ is the contribution of the $i-$th spring, d_i is the local penetration in the body, and G is the shear elastic modulus. Similarly, the contribution of a single damper can be found by substituting position with velocity and elasticity with viscosity, i.e., in (2) $d \to \dot{d}$ and $G \to \eta$, thus obtaining

$$f_{M,i} = 4\eta \dot{d}_i \Delta x, \tag{3}$$

where $\dot{d}_i$ is the velocity of penetration and η is the viscosity of the material. Integrating the sum of (2) and (3) with $\Delta x \to 0$ and approximating the circular arc by a parabola (as per the Hertzian theory), we obtain that the force action generated by the material on the end-effector is given by

$$F_M(d) = \begin{cases} \kappa d^{\frac{3}{2}} + \lambda d^{\frac{1}{2}} \dot{d}, & d \geq 0, \\ 0 & d < 0, \end{cases} \tag{4}$$

where the new model parameters κ and λ for an incompressible viscoelastic material are

$$\kappa = \frac{16G}{3}\sqrt{r} \text{ and } \lambda = 8\eta\sqrt{r}. \tag{5}$$

Using (4), it is therefore possible to model nonlinear effects in the contact without having to estimate the material-specific value of the exponent of the HC model. The complete derivation can be found in [19], [20].

A. Online Estimation with Measured Force Inputs

The force measured by a force sensor positioned on the robot's end effector can be written as the sum of the force generated by the soft tissue and the inertia of the indenter. For the sake of simplicity, we will explain the formulation first with the Kelvin-Voigt model, and then adapt it with the DRM method. Using the simpler KV model (1), the force on the end-effector in contact with a soft surface can be written as

$$F_{FT} = k_M d + c_M \dot{d} + m_I \ddot{d}, \tag{6}$$

where m_I is the mass of the indenter attached to the force sensor. Solving (6) for $\ddot{d}$, we obtain the differential equation

$$\ddot{d} = \frac{1}{m_I}\left(F_{FT} - k_M d - c_M \dot{d}\right),$$

from which it is easy to derive a state space representation of the dynamical system. The state vector $\boldsymbol{x} \in \mathbb{R}^4$ is defined, which contains the penetration inside the body, the velocity of the indenter, the stiffness, and the damping of the soft tissue, $\boldsymbol{x} = \left[d, \dot{d}, k_M, c_M\right]^\top$. The corresponding discrete-time model, $\boldsymbol{x}_{t+1} = f_t(\boldsymbol{x}_t, u_t, \boldsymbol{w}_t)$, assuming ΔT as sampling time, is

$$\begin{aligned} x_{1,t+1} &= x_{1,t} + \Delta T x_{2,t} + w_1, \\ x_{2,t+1} &= x_{2,t} + \frac{\Delta T}{m_I}\left(u_t - x_{1,t}x_{3,t} - x_{2,t}x_{4,t}\right) + w_2, \\ x_{3,t+1} &= x_{3,t}, \\ x_{4,t+1} &= x_{4,t}. \end{aligned} \tag{7}$$

The input of the system u_t is the force F_{FT} measured by the F/T sensor, $\boldsymbol{x}_t$ is the state at the current time step, $\boldsymbol{x}_{t+1}$ is the state at the following time step and $\boldsymbol{w}_t$ is the model noise, which is assumed to be i.i.d zero mean Gaussian process $w_t \sim \mathcal{N}(\mathbf{0}, \mathbf{Q})$, with $\mathbf{Q} = diag\left(\sigma_{x_1}^2, \sigma_{x_2}^2\right)$. It can be observed from (7) that the stiffness and damping coefficients are time-invariant, so no model uncertainty is considered in their dynamics. Moreover, since the integration time interval ΔT is very small, we assumed the velocity to be constant in ΔT. Furthermore, since the robot end-effector is always in contact during the estimation phase, the velocity of the indenter inside the soft body is the same as the velocity of the end effector. The quantity can be calculated by utilising the velocity of the robot's joint and the Jacobian matrix through direct differential kinematics. The measurement function $z_t = h_t(\boldsymbol{x}_t, v_t)$, instead, can be defined

$$z_t = x_{2,t} + v_t, \tag{8}$$

where v_t is the measurement uncertainty, which is assumed to be an i.i.d. zero mean Gaussian process $v_t \sim \mathcal{N}(0, \sigma_v^2)$.

The same procedure can be followed substituting the nonlinear model in (4) in (6), obtaining a new update rule for the velocity of the end-effector. The state vector is in this case $\boldsymbol{x} = \left[d, \dot{d}, \kappa, \lambda\right]$, and the velocity update rule is

$$x_{2,t+1} = x_{2,t} + \frac{\Delta T}{m_I}\left(u_t - x_{1,t}^{\frac{3}{2}}x_{3,t} - x_{1,t}^{\frac{1}{2}}x_{2,t}x_{4,t}\right) + w_2. \tag{9}$$

B. Online Sensorless Estimation with Force Approximation

The following section presents a method for estimating the soft tissue parameters without a 6-axis force sensor. The method is underlined by the observation that the interaction force of the robot with the environment, generated by a Cartesian impedance controller, is in general equal to the external forces measured by the F/T sensor. Hence, in the above-mentioned conditions, it is possible to exploit a Cartesian impedance controller to estimate the interaction forces without having a force torque sensor mounted on the end effector. A similar approach has been proposed by Roveda et al. in static conditions [17]. However, in this approach, the impedance control law is equated to the force generated by a spring neglecting the damping term and the equilibrium position is evaluated prior to the elastic estimation with a strict procedure which requires the robot to be positioned in close proximity to the contact surface.

In a Cartesian impedance controller, the physical interaction of the end-effector with the environment $\boldsymbol{F}_{ee}^{ext}$ approximates a mass-spring-damper system with desired parameters

$$\boldsymbol{\Lambda}_d \ddot{\tilde{\boldsymbol{x}}}_{ee} + \boldsymbol{D}_d \dot{\tilde{\boldsymbol{x}}}_{ee} + \boldsymbol{K}_d \tilde{\boldsymbol{x}}_{ee} = \boldsymbol{F}_{ee}^{ext}, \tag{10}$$

where $\tilde{\boldsymbol{x}}_{ee} = \boldsymbol{x}_d - \boldsymbol{x}_{ee} \in \mathbb{R}^m$ is the Cartesian position error $\boldsymbol{x}_d$, $\boldsymbol{\Lambda}_d \in \mathbb{R}^{m\times m}$, $\boldsymbol{D}_d \in \mathbb{R}^{m\times m}$ and $\boldsymbol{K}_d \in \mathbb{R}^{m\times m}$ are the desired Cartesian inertia, damping, and stiffness, respectively. In general, the implementation of a closed-loop scheme to render the behaviour in (10) requires a force/torque sensor capable of measuring $\boldsymbol{F}_{ee}^{ext}$. However, under the assumption of natural inertia $\boldsymbol{\Lambda}_d = \boldsymbol{\Lambda}(\boldsymbol{x})$, the feedback of external forces can be avoided [22]. The control law in (10) can be reformulated as

$$\boldsymbol{\Lambda}(\boldsymbol{x}) \ddot{\tilde{\boldsymbol{x}}}_{ee} + \boldsymbol{D}_d \dot{\tilde{\boldsymbol{x}}}_{ee} + \boldsymbol{K}_d \tilde{\boldsymbol{x}} = \boldsymbol{F}_{ee}^{ext}. \tag{11}$$

As discussed in Section II-A, also in this case we will start by formulating the estimation model using the linear KV model. Since the force measured by the F/T sensor is equivalent to the force generated by the impedance controller, to estimate the force acting on the material, we can equate (6) with (11) in the contact direction. Assuming that the contact occurs in the z-direction, we can extract an equation in such a direction from the general equation (11). Given $\boldsymbol{\Lambda}(x) = [\Lambda_{ij}]$, $\boldsymbol{D}_d = [D_{ij}]$ and $\boldsymbol{K}_d = [K_{ij}]$, the resulting equation is as follows

$$\Lambda_{33}\ddot{\tilde{z}} + D_{33}\dot{\tilde{z}} + K_{33}\tilde{z} = k_M d + c_M \dot{d} + m_I \ddot{d}. \tag{12}$$

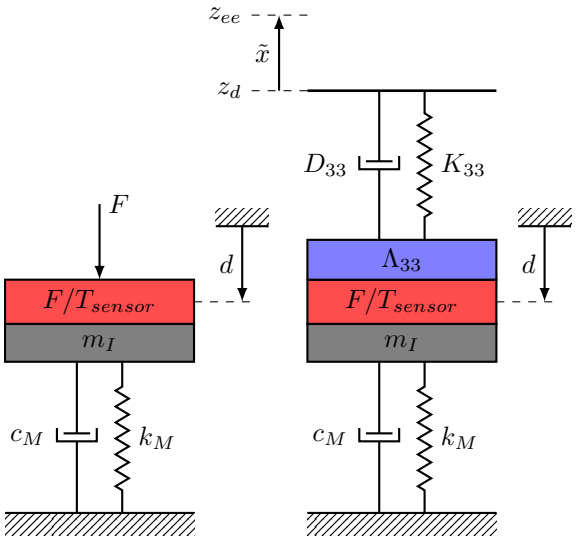

Fig. 2. The left model represents the system described in (7), where it is assumed that a force is acting on the F/T sensor. The sensor is connected to a mass, which is in turn connected to a spring-damper element. The model described in (15) is shown on the right, where the impedance control model is displayed instead of the external force.

As the robot end-effector is in contact with the material, we have $\dot{z}_e = -\dot{d}$ and $\ddot{z}_e = -\ddot{d}$. Using this information we can rewrite (12) as

$$\Lambda_{33}(\ddot{z}_d + \ddot{d}) + D_{33}(\dot{z}_d + \dot{d}) + K_{33}\tilde{z} + k_M d + c_M \dot{d} + m_I \ddot{d} = 0, \tag{13}$$

and, finally, solving (13) for $\ddot{d}$ to obtain

$$\ddot{d} = -\frac{1}{m_I + \Lambda_{33}} \Big(\Lambda_{33}\ddot{z}_d + D_{33}\dot{z}_d + K_{33}\tilde{z} + (D_{33} + c_M)\dot{d} + k_M d \Big). \tag{14}$$

Using (14) we can write the new discrete-time model of the system. The input now becomes $\boldsymbol{u} = [\tilde{z}, \dot{z}_d, \ddot{z}_d, \Lambda_{33}]^T \in \mathbb{R}^4$. The new discrete time model $\boldsymbol{x}_{t+1} = f(\boldsymbol{x}_t, \boldsymbol{u}_t, \boldsymbol{w}_t)$ is the same as in (7) except for the definition of $x_{2,t+1}$, redefined as

$$x_{2,t+1} = x_{2,t} - \frac{\Delta T}{m_I + u_{4,t}} (u_{4,t}u_{3,t} + D_{33}u_{2,t} + K_{33}u_{1,t} + x_{3,t}x_{1,t} + (D_{33} + x_{4,t})x_{2,t}) + w_{2,t}. \tag{15}$$

Similarly, the measurement function (8) remains the same.

The model can be interpreted as two masses, each connected to a spring-damper set, and rigidly connected to one another, as shown in Fig. 2. The first spring-damper element represents the force generated by the impedance controller, with the desired position as input. The mass of the impedance controller and the indenter are divided by the force sensor, which measures all the forces acting on the end-effector. Finally, the second spring-damper element represents the force generated by the soft tissue.

Again, the update of the penetration velocity (15) can be rewritten using the DRM in (4) as

$$x_{2,t+1} = x_{2,t} - \frac{\Delta T}{m_I + u_{4,t}} (u_{4,t}u_{3,t} + D_{33}u_{2,t} + K_{33}u_{1,t} + x_{1,t}^{\frac{3}{2}}x_{3,t} + x_{1,t}^{\frac{1}{2}}x_{2,t}x_{4,t} + D_{33}x_{2,t}) + w_{2,t}. \tag{16}$$

C. Extended Kalman Filter

The system unknown variables (both static and dynamic) can be estimated using an extended Kalman filter (EKF). This filter corrects the update of a given model using the information provided by a measurement. Each step of the filter is composed of two phases: the update phase and the correction phase. In the update phase, the previous values are used to compute the new ones

$$\hat{\boldsymbol{x}}_{t+1}^- = f(\hat{\boldsymbol{x}}_t, \boldsymbol{u}_t, \boldsymbol{w}_t),$$
$$\boldsymbol{P}_{t+1}^- = \boldsymbol{A}_t \boldsymbol{P}_t \boldsymbol{A}_t^T + \boldsymbol{G}_t \boldsymbol{Q}_t \boldsymbol{G}_t^T,$$

where $\boldsymbol{A_t}$ and $\boldsymbol{G_t}$ are respectively the gradient of f with respect to $\boldsymbol{x}$ and $\boldsymbol{w}$ computed in $[\hat{\boldsymbol{x}}_t, \boldsymbol{u}_t, \mathrm{E}\{\boldsymbol{w}_t\}]$, where $\mathrm{E}\{\boldsymbol{w}_t\} = 0$ is the expected value (mean) of the uncertainties. $\boldsymbol{Q}_t$ is the possibly time varying covariance matrix of the uncertainties $\boldsymbol{w}$, while $\boldsymbol{P}_t$ is the customary covariance matrix of the estimation error. For the correction step, we have

$$\boldsymbol{S}_{t+1} = \boldsymbol{H}_{t+1} \boldsymbol{P}_{t+1}^- \boldsymbol{H}_{t+1}^T + \boldsymbol{R}_{t+1},$$
$$\boldsymbol{W}_{t+1} = \boldsymbol{P}_{t+1}^- \boldsymbol{H}_{t+1}^T \boldsymbol{S}_{t+1}^{-1},$$
$$\hat{\boldsymbol{x}}_{t+1} = \hat{\boldsymbol{x}}_{t+1}^- \boldsymbol{W}_{t+1}(\boldsymbol{x}_{t+1} - h(\hat{\boldsymbol{x}}_{t+1}^-, v_{t+1})),$$
$$\boldsymbol{P}_{t+1} = (\boldsymbol{I} - \boldsymbol{W}_{t+1}\boldsymbol{H}_{t+1})\boldsymbol{P}_{t+1}^-,$$

where $\boldsymbol{H}_{t+1}$ is the gradient of h in respect to x computed in $\left[\hat{\boldsymbol{x}}_{t+1}^-, \mathrm{E}\{v_{t+1}\}\right]$, where, again, $\mathrm{E}\{v_{t+1}\} = 0$. Finally, $\boldsymbol{R}_{t+1}$ is the possibly time varying covariance matrix of the additive uncertainties v_{t+1}.

III. EXPERIMENTS

The feasibility of the estimation algorithm for penetration, stiffness, and damping of soft bodies made of different silicone materials is here discussed. To this end, a sinusoidal desired trajectory is imposed on the impedance controller to obtain the maximum information from the palpation,

$$z_d(t) = z_0 + z_1 \sin(4\pi t) + z_2 \sin(8\pi t). \tag{17}$$

The experiments used a 6-DoF position-controlled robotic arm, specifically the UR3e showed in Fig. 3a. The robot's end-effector was equipped with a force torque sensor and a 3D-printed indenter. The 6-axis Bota SensOne was used as force sensor and the indenter's tip is shaped as a 2 cm diameter spherical cap. The communication between the robot and control was achieved using ROS2 Humble. A controller that simulates the behaviour of a torque-controlled robot was used since the robot is position-controlled and does not expose any interface for joint torque inputs [23]. The control law (11) has been simplified by neglecting the noisy contribution of the acceleration, resulting in

$$-\boldsymbol{D}_d \dot{\boldsymbol{x}}_{ee} + \boldsymbol{K}_d \tilde{\boldsymbol{x}}_{ee} \approx \boldsymbol{F}_{ee}^{ext}, \tag{18}$$

(a) (b)

Fig. 3. (a) The experimental setup is composed of a position-controlled Ur3e, a 6-axis force torque sensor BOTA SensorONe, a 3D printed indenter and a silicone specimen. (b) The 4 types of silicone. S1 is softer (ECOFLEX-0030), S2 is the soft silicone with a steel ball, S3 refers to the stiffer silicone (Dragonskin-10NV) and S4 is the same silicone as S3 with a steel ball.

therefore implying the adaptation of (15) and (16). During the experiments, the translational stiffness of the control was set to $K_{ii} = 1000\,\mathrm{Nm}^{-1}$ and the translational damping to $D_{ii} = 2\sqrt{1000}\,\mathrm{Nsm}^{-1}$ with $i = \{1, 2, 3\}$.

Specimens were fabricated using two types of silicone with different stiffness: Dragonskin-10NV, which is stiffer and similar to muscles, and ECOFLEX-0030, which is softer and similar to fat [24]. The same moulding procedure was used to manufacture all specimens. Firstly, the two liquid reacting components were mixed, and then the mixture was put in a vacuum chamber for degassing. The mould used was a cylinder with a diameter of $5\,\mathrm{cm}$ and a height of $2.1\,\mathrm{cm}$. In addition to pure silicone specimens, we created silicone specimens with a metal sphere inside to simulate a tissue containing cancerous cells. The metal sphere, with a diameter of $9\,\mathrm{mm}$, was inserted into the liquid mixture after the degassing phase. Since cancerous tissue can be up to 100 times stiffer than healthy tissue, we believe that the use of a metallic inclusion provides a good benchmark for our application [25]. In the manufactured specimens, the sphere sits at a distance of about $1\,\mathrm{cm}$ from the bottom surface. The four specimens used during the experiments are shown in Fig. 3b. In the following discussion of the experiments, some abbreviations have been used:

- R refers to the reference values computed offline with a least squares method;
- M_1 refers to the first model (7) where the KV and the F/T sensor are used;
- M_2 refers to the second model (15) where the KV and the impedance control are used;
- M_3 refers to the third model (9) where the DRM and the F/T sensor are used;
- M_4 refers to the fourth model (16) where the DRM and the impedance control are used.

Silicone samples will be referred to with the abbreviations defined in Fig. 3b, i.e., S1 to S4. To ensure a fair comparison, all tests were conducted using the same filter initial condition $\hat{\boldsymbol{x}}_0 = [1, 1, 0, 0]$ and the same initial covariance matrix $\boldsymbol{P}_0$, equal to an identity matrix. The four algorithms were executed on the data obtained from a single measurement for each specimen.

A. Models Validation

Figure 4 shows the behaviour of the EKF with the different types of models. For sake of space, we only report the results obtained for the harder silicone sample, S1, as other samples behaviour and thus considerations are reasonably similar. The reference values are calculated by determining the precise location of the soft body's surface and using the least squares method to identify the stiffness and damping values that minimise the sum of the residuals. The 4 plots in the first row refer to models M_1 and M_2: upon examining the penetration, it is evident that the estimated value of x_1 converges to a lower value than the actual one, regardless of whether the F/T sensor is used. Additionally, the stiffness value x_3 converges to a higher value than the actual one. This discrepancy is due to the inaccurate description of the system dynamics by the KV model, failing state values to converge to the actual values.

The four plots in the second row refer to the models M_3 and M_4: the penetration x_1 and the stiffness x_3 are now converging to their expected values, as the velocity and viscosity do quite rapidly. This is because the velocity is directly measured and corrected within the EKF.

Upon examination of the plots, it becomes evident that the necessity for exploiting a novel model capable of accurately describing contact behaviour arises. With the DRM, differently from the KV model, the filter can converge to the correct values.

B. Force Reconstruction

As the identification procedure can be performed without a force sensor, it is worth investigating how well the force can be reconstructed using the estimated parameters. In Fig. 5 the comparison between the measured force and the reconstructed forces is shown; again, the behaviour of only the harder sample (S1) is shown. We can notice that after

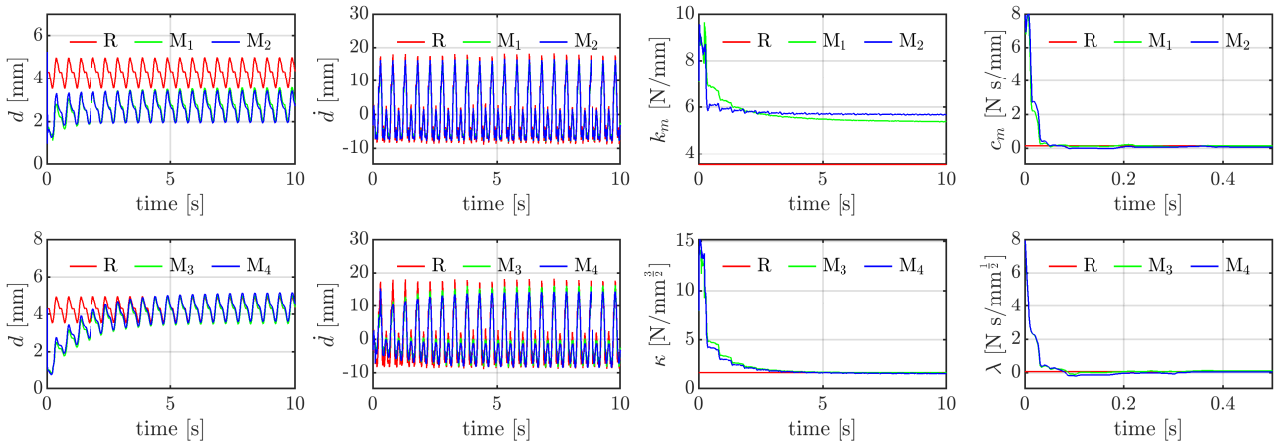

Fig. 4. Results of the states estimation using the developed models with the softer silicone S1. In red with the label R are plotted the reference values computed with the LS method. In the first row are shown the results using the Kelvin-Voigt model with and without force sensor (M_1 and M_2). The second row shows the results of the estimation using the DRM to model the soft body with and without the force torque sensor (M_3 and M_4).

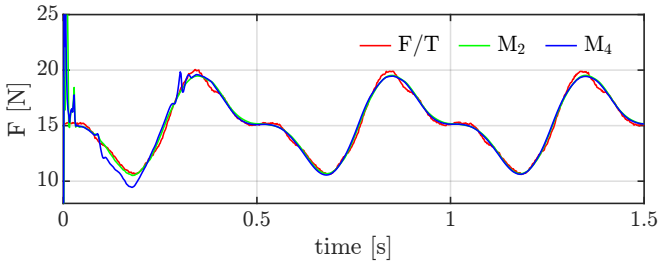

Fig. 5. Comparison of the measured forces (F/T in red) against the estimated ones (M_2 in green and M_4) without the use of the sensor.

the initial 30 ms the force computed with M_2 and M_4 has an absolute error of 0.4 N. The mean squared error (MSE) computed between 5 s and 10 s, which is a reasonable time for filter convergence, is equal to $0.0614\,\mathrm{N}^2$ for M_2 and to $0.0559\,\mathrm{N}^2$ for M_4. Despite converging to incorrect values, model M_2 can precisely track the force that is acting on the end-effector. This demonstrates the theoretical possibility of using the robot without a force sensor and still accurately determining the force on the end-effector. It is worth noting that the estimated force is ahead of the measured force. This is because the robot is not torque-controlled, but instead uses a control that mimics the operation of an impedance control [15], thus inducing a delay in the control chain.

C. Tumour Identification

A sinusoidal palpation was performed for each silicone, whose results are reported in Tab. I. As expected from Fig. 4, the first two models, M_1 and M_2, do not converge to the correct stiffness. The filer convergence speed is in the order of some seconds; there are negligible differences between the values found at 5 s and 10 s. Despite limited accuracy in the estimates, we acknowledge a variation between the parameter values of the silicones with and without the steel ball, so it is theoretically possible to use such values to detect the potential presence of foreign masses. For example, it is possible to compare the estimate of the diseased tissue with the estimate of the same healthy tissue in the vicinity. In that case, a difference in the model stiffness value can be recognised. Models M_3 and M_4, on the other hand, have slower dynamics but they converge to the correct value of stiffness and damping, thus ensuring the detection of the silicone containing the metal ball. Models M_2 and M_4, which use the impedance controller instead of the force sensor, tend to converge to lower values of the stiffness. The reason for this mismatch is that the impedance model within the EKF is just an approximation of the law that controls the robot. As explained before, it is due to the presence of a position control which only mimics an impedance behaviour. Despite this drawback, the different values still allow us to distinguish the different materials.

IV. CONCLUSIONS

This paper demonstrates the possibility of estimating soft tissue characteristics and end-effector penetration using dimensionality reduction and an extended Kalman filter. The filter also allows for the estimation of end-effector forces without the need for additional sensors. The experiments demonstrated the fast convergence of the filter and the accurate estimation of parameters for materials with different elasticity and viscosity, which makes it suitable for applications which require rapid, but accurate, contact information. In addition, we investigated the capability of the method to detect stiffer foreign bodies within soft materials. The results showed that elements with diameters smaller than 1 cm were consistently found in multiple experiments with different types of silicone.

Although we were able to estimate the desired properties, further studies are required. Firstly, a method to estimate the depth of hard intrusions would also benefit medical professionals. Secondly, the limitations of the method in detecting smaller intrusions should be highlighted. One potential solution to these shortcomings is to merge the tactile estimation data with information gathered from an ultrasound scanner. Finally, one might be interested in analysing the

TABLE I

RESULTS OF THE ESTIMATION OF x_3 AND x_4 FOR EACH MODEL OBTAINED OVER THE SAME DATASET FOR EACH SAMPLE TYPE AFTER 5 AND 10 SECONDS OF PALPATION.

SILICONE	MODEL	TIME	ESTIMATION		REFERENCE		ERROR 10S	
[#]	[#]	[s]	x_3 [$\mathrm{Nmm}^{-\frac{3}{2}}$]	x_4 [$\mathrm{Nsmm}^{-\frac{1}{2}}$]	x_3 [$\mathrm{Nmm}^{-\frac{3}{2}}$]	x_4 [$\mathrm{Nsmm}^{-\frac{1}{2}}$]	e_3 [%]	e_4 [%]
S_1	M_1	5/10	3.45/3.41	0.099/0.098	2.03	0.093	68	5
S_2	M_1	5/10	4.51/4.37	0.120/0.118	2.49	0.118	76	0
S_3	M_1	5/10	5.49/5.38	0.159/0.159	3.53	0.160	52	1
S_4	M_1	5/10	6.88/6.85	0.119/0.119	4.19	0.121	63	2
S_1	M_2	5/10	3.39/3.31	0.130/0.130	2.03	0.093	63	40
S_2	M_2	5/10	4.48/4.25	0.118/0.122	2.49	0.118	71	3
S_3	M_2	5/10	5.33/5.29	0.118/0.118	3.53	0.160	50	26
S_4	M_2	5/10	6.45/6.45	0.025/0.026	4.19	0.121	54	79
SILICONE	MODEL	TIME	ESTIMATION		REFERENCE		ERROR 10S	
[#]	[#]	[s]	x_3 [$\mathrm{Nmm}^{-\frac{3}{2}}$]	x_4 [$\mathrm{Nsmm}^{-\frac{1}{2}}$]	x_3 [$\mathrm{Nmm}^{-\frac{3}{2}}$]	x_4 [$\mathrm{Nsmm}^{-\frac{1}{2}}$]	e_3 [%]	e_4 [%]
S_1	M_3	5/10	0.961/0.877	0.040/0.039	0.742	0.038	18	5
S_2	M_3	5/10	2.40/1.27	0.047/0.053	1.01	0.052	25	2
S_3	M_3	5/10	1.76/1.70	0.082/0.078	1.70	0.081	0	4
S_4	M_3	5/10	2.53/2.46	0.068/0.066	2.18	0.069	13	4
S_1	M_4	5/10	0.856/0.791	0.060/0.056	0.742	0.038	7	47
S_2	M_4	5/10	1.30/1.16	0.069/0.064	1.01	0.052	15	23
S_3	M_4	5/10	1.69/1.61	0.071/0.070	1.70	0.081	5	13
S_4	M_4	5/10	2.29/2.16	0.044/0.048	2.18	0.069	1	30

effect of different impedance control parameters, such as stiffness, on the filter performance.

REFERENCES

[1] P. Dario and M. Bergamasco, "An advanced robot system for automated diagnostic tasks through palpation," *IEEE Trans Biomed Eng*, vol. 35, no. 2, pp. 118–126, 1988.

[2] N. Herzig, P. Maiolino, F. Iida, and T. Nanayakkara, "A Variable Stiffness Robotic Probe for Soft Tissue Palpation," *IEEE Robotics and Automation Letters*, vol. 3, no. 2, pp. 1168–1175, 4 2018.

[3] L. Scimeca, P. Maiolino, E. Bray, and F. Iida, "Structuring of tactile sensory information for category formation in robotics palpation," *Autonomous Robots*, vol. 44, no. 8, pp. 1377–1393, 11 2020.

[4] E. Samur, M. Sedef, C. Basdogan, L. Avtan, and O. Duzgun, "A robotic indenter for minimally invasive measurement and characterization of soft tissue response," *Med Image Anal*, vol. 11, no. 4, pp. 361–373, 8 2007.

[5] B. Ahn, Y. Kim, C. K. Oh, and J. Kim, "Robotic palpation and mechanical property characterization for abnormal tissue localization," *Medical and Biological Engineering and Computing*, vol. 50, no. 9, pp. 961–971, 9 2012. [Online]. Available: https://link.springer.com/article/10.1007/s11517-012-0936-2

[6] Y. P. Zheng and A. F. Mak, "An ultrasound indentation system for biomechanical properties assessment of soft tissues in-vivo," *IEEE Transactions on Biomedical Engineering*, vol. 43, no. 9, 1996.

[7] L. Barbé, B. Bayle, M. De Mathelin, and A. Gangi, "In vivo model estimation and haptic characterization of needle insertions," in *International Journal of Robotics Research*, vol. 26, no. 11-12, 2007.

[8] K. Hashtrudi-Zaad and S. E. Salcudean, "Adaptive transparent impedance reflecting teleoperation," in *Proceedings - IEEE International Conference on Robotics and Automation*, vol. 2, 1996.

[9] L. J. Love and W. J. Book, "Force reflecting teleoperation with adaptive impedance control," *IEEE Transactions on Systems, Man, and Cybernetics, Part B (Cybernetics)*, vol. 34, no. 1, pp. 159–165, 2004.

[10] R. Cortesão, J. Park, and O. Khatib, "Real-time adaptive control for haptic telemanipulation with kalman active observers," *IEEE Transactions on Robotics*, vol. 22, no. 5, pp. 987–999, 2006.

[11] L. Beber, E. Lamon, D. Nardi, D. Fontanelli, M. Saveriano, and L. Palopoli, "A Passive Variable Impedance Control Strategy with Viscoelastic Parameters Estimation of Soft Tissues for Safe Ultrasonography," *IEEE International Conference on Robotics and Automation (ICRA)*, pp. 1298–1304, 5 2024.

[12] A. Pappalardo, A. Albakri, C. Liu, L. Bascetta, E. De Momi, and P. Poignet, "Hunt-Crossley model based force control for minimally invasive robotic surgery," *Biomedical Signal Processing and Control*, vol. 29, 2016.

[13] K. H. Hunt and F. R. E. Crossley, "Coefficient of restitution interpreted as damping in vibroimpact," 1975.

[14] N. Diolaiti, C. Melchiorri, and S. Stramigioli, "Contact impedance estimation for robotic systems," *IEEE Transactions on Robotics*, vol. 21, no. 5, pp. 925–935, 10 2005.

[15] R. Schindeler and K. Hashtrudi-Zaad, "Online Identification of Environment Hunt-Crossley Models Using Polynomial Linearization," *IEEE Transactions on Robotics*, vol. 34, no. 2, 2018.

[16] X. Zhu, B. Gao, Y. Zhong, C. Gu, and K. S. Choi, "Extended Kalman filter for online soft tissue characterization based on Hunt-Crossley contact model," *Journal of the Mechanical Behavior of Biomedical Materials*, vol. 123, 2021.

[17] L. Roveda, A. A. Shahid, N. Iannacci, and D. Piga, "Sensorless Optimal Interaction Control Exploiting Environment Stiffness Estimation," *IEEE Transactions on Control Systems Technology*, 2022.

[18] X. Zhu, J. Li, Y. Zhong, K. S. Choi, B. Shirinzadeh, J. Smith, and C. Gu, "Iterative Kalman filter for biological tissue identification," *International Journal of Robust and Nonlinear Control*, 2023.

[19] V. L. Popov and M. Heß, *Method of dimensionality reduction in contact mechanics and friction*. Springer, 2015.

[20] L. Beber, E. Lamon, L. Palopoli, L. Fambri, M. Saveriano, and D. Fontanelli, "Elasticity Measurements of Expanded Foams Using a Collaborative Robotic Arm," *IEEE Instrumentation and Measurement Technology Conference (I2MTC)*, 2024.

[21] M. S. Sacks and W. Sun, "Multiaxial mechanical behavior of biological materials," *Annual Review of Biomedical Engineering*, vol. 5, 2003.

[22] A. Dietrich, X. Wu, K. Bussmann, M. Harder, M. Iskandar, J. Englsberger, C. Ott, and A. Albu-Schäffer, "Practical consequences of inertia shaping for interaction and tracking in robot control," *Control Engineering Practice*, vol. 114, p. 104875, 9 2021.

[23] S. Scherzinger, A. Roennau, and R. Dillmann, "Forward Dynamics Compliance Control (FDCC): A new approach to cartesian compliance for robotic manipulators," *IEEE International Conference on Intelligent Robots and Systems*, pp. 4568–4575, 12 2017.

[24] J. L. Sparks, N. A. Vavalle, K. E. Kasting, B. Long, M. L. Tanaka, P. A. Sanger, K. Schnell, and T. A. Conner-Kerr, "Use of silicone materials to simulate tissue biomechanics as related to deep tissue injury," *Advances in skin & wound care*, vol. 28, no. 2, pp. 59–68, 2015.

[25] R. Nadan, H. Irena, O. Milorad, O. Rajko, J. R. Jasminka, K. Marino, P. Roland, and V. Boris, "EUS elastography in the diagnosis of focal liver lesions," *Gastrointestinal Endoscopy*, vol. 66, no. 4, 2007.